Received: 8 December 2022 | Revised: 5 February 2023 | Accepted: 21 February 2023

DOI: 10.1002/psc.3486

RESEARCH ARTICLE

Journal of PeptideScience WILEY

Effect of macrocyclization and tetramethylrhodamine labeling on chemokine binding peptides

Julia S. Wack[1] | Kevin Brahm[1] | Philipp Babel[2] | James A. R. Dalton[3,4] | Katja Schmitz[1]

[1]Biological Chemistry, Clemens-Schöpf-Institute for Organic Chemistry and Biochemistry, Technical University of Darmstadt, Darmstadt, Germany

[2]Computational Biology and Simulation, Technical University of Darmstadt, Darmstadt, Germany

[3]Laboratory of Molecular Neuropharmacology and Bioinformatics, Unitat de Bioestadística, Institut de Neurociències, Universitat Autònoma de Barcelona, Bellaterra, Spain

[4]Ronin Institute, Montclair, New Jersey, USA

Correspondence
Katja Schmitz, Biological Chemistry, Clemens-Schöpf-Institute for Organic Chemistry and Biochemistry, Technical University of Darmstadt, Alarich-Weiss-Str. 8, D-64287 Darmstadt, Germany.
Email: katja.schmitz@tu-darmstadt.de

Receptor-derived peptides have played an important role in elucidating chemokine-receptor interactions. For the inflammatory chemokine CXC-class chemokine ligand 8 (CXCL8), a site II-mimetic peptide has been derived from parts of extracellular loops 2 and 3 and adjacent transmembrane helices of its receptor CXC-class chemokine receptor 1 (Helmer et al., *RSC Adv*., 2015, **5**, 25657). The peptide sequence with a C-terminal glutamine did not bind to CXCL8, whereas one with a C-terminal glutamate did but with low micromolar affinity. We sought to improve the affinity and protease stability of the latter peptide through cyclization while also cyclizing the former for control purposes. To identify a cyclization strategy that permits a receptor-like interaction, we conducted a molecular dynamics simulation of CXCL8 in complex with full-length CXC-class chemokine receptor 1. We introduced a linker to provide an appropriate spacing between the termini and used an on-resin side-chain-to-tail cyclization strategy. Upon chemokine binding, the fluorescence intensity of the tetramethylrhodamine (TAMRA)-labeled cyclic peptides increased whereas the fluorescence anisotropy decreased. Additional molecular dynamics simulations indicated that the fluorophore interacts with the peptide macrocycle so that chemokine binding leads to its displacement and observed changes in fluorescence. Macrocyclization of both 18-amino acid-long peptides led to the same low micromolar affinity for CXCL8. Likewise, both TAMRA-labeled linear peptides interacted with CXCL8 with similar affinities. Interestingly, the linear TAMRA-labeled peptides were more resistant to tryptic digestion than the unlabeled counterparts, whereas the cyclized peptides were not degraded at all. We conclude that the TAMRA fluorophore tends to interact with peptides altering their protease stability and behavior in fluorescence-based assays.

KEYWORDS
binding assay, chemokine-receptor interaction, peptide macrocycles, stability, TAMRA labeling

Abbreviations: Ahx, aminohexanoic acid; Alloc, allyloxycarbonyl; CD, circular dichroism; COM, center of mass; CV, column volume; CXCL8, CXC-class chemokine ligand 8 (interleukin 8); CXCR1, CXC-class chemokine receptor 1 (IL8RA); DCM, dichloromethane; DIPEA, *N,N* -diisopropylethylamine; DMF, dimethyl formamide; ECL, extracellular loop; HBTU, 2-(1*H*-benzotriazol-1-yl)-1,1,3,3-tetramethyluronium hexafluorophosphate; MD, molecular dynamics; Mtt, 4-methyltrityl; RMSD, root mean square deviation; RMSF, root mean square fluctuation; TAMRA, tetramethylrhodamine; TFA, trifluoroacetic acid; TM, transmembrane helix.

Julia S. Wack, Kevin Brahm, and Philipp Babel contributed equally to this article.

1 | INTRODUCTION

Peptides derived from ligand-binding sites are useful tools to study protein–protein interactions.[1,2] They can be used to elucidate biochemical pathways, detect proteins in diagnostic applications, or inhibit protein functions involved in diseases.[3–5] Chemokine receptors, a class of G protein-coupled receptors, are involved in the migration of immune cells in inflammation and homeostasis of the immune system.[6] Peptides derived from respective receptor sequences have been frequently used to investigate chemokine-receptor interactions.[7] Chemokines bind to their receptor by a two-site mechanism, in which the receptor's N-terminus (chemokine recognition site I) binds to the chemokine and the chemokine's N-terminus binds to a region defined by extracellular loops (ECLs) and transmembrane helices, referred to as "site II";[8,9] or chemokine recognition site 2.[10] Peptides derived from the receptor's N-terminus have played an important role in the elucidation of this mechanism (see Szpakowska et al.[7] for a review). Mimicking site II is more demanding considering its location on discontinuous peptide sequences with essential amino acids located in different ECLs and adjacent transmembrane helices of the GPCR.[6,8]

Synthetic peptides derived from the ECLs of CCR5, the receptor of RANTES/CCL5 and coreceptor for HIV-entry into T-cells, inhibited binding of HIV envelope glycoprotein gp120 to CCR5 and prevented infection with HIV strains that recognize CCR5.[11] A series of synthetic peptide-based mimetics of receptor CXCR4 have been developed to target gp120.[12] It was shown by Eichler et al. that a fusion peptide of ECL1 to ECL3 and derivatives thereof exhibit high affinity toward gp120 and inhibit infection with X4 tropic strains of the human immunodeficiency virus (HIV).[12] Interestingly, a peptide derived from ECL2 not only inhibited viral entry at a moderate level but also inhibited binding of chemokine CXCL12 to CXCR4. At the same time, Chevigne et al. showed that a CXCR4–ECL2-derived peptide interacts with CXCL12 with a dissociation constant of 22 nM and can be considered a receptor mimetic.[10] In our previous work, we developed a peptide mimicking site II of the CXCL8 receptor CXCR1.[13] This peptide, IL8RP-Loops, comprises sequences from ECL2 and ECL3 and adjacent transmembrane helices (TM5 and TM6), namely, A196 to I204 (ECL2/TM5) and A264 to Q271 (TM6/ECL3). These two peptides were connected by a flexible aminohexanoic acid (Ahx) linker that corresponds to the distance between TM5 and TM6 measured between the α-carbons of I204 and A264 (10.73 Å measured in protein data bank (PDB) structure 2LNL; see Figure 1A). This peptide was able to bind the chemokine ligand CXCL8 with ~1-μM affinity and inhibited biological responses of CXCL8 such as receptor internalization and chemotaxis.[13] Further investigations by high-resolution mass spectrometry[16] revealed that glutamic acid had been incorporated as the C-terminal residue instead of glutamine. We assumed that under the alkaline conditions during cleavage of the peptide from the resin in the previous work, a glutarimide formed at the C-terminal position was subsequently hydrolyzed to glutamic acid.[17] No affinity of IL8RP-LoopsQ to CXCL8 could be detected by fluorescence polarization, and IL8RP-LoopsE exhibited low micromolar affinity.[16] Cyclization leads to a more rigid structure and reduces the entropic penalty as the peptide binds to its target protein and thereby lowers the free binding energy.[18–21] It is also a common approach to improve protease stability of peptides.[22–24] Therefore, we cyclized IL8RP-LoopsE to improve its properties. IL8RP-LoopsQ was cyclized as a control.

2 | MATERIALS AND METHODS

All chemicals and materials used in this work were procured from the companies below, if not stated otherwise: AB SCIEX (Framingham, MA, USA), AppliChem GmbH (Darmstadt, DE), Carbolution

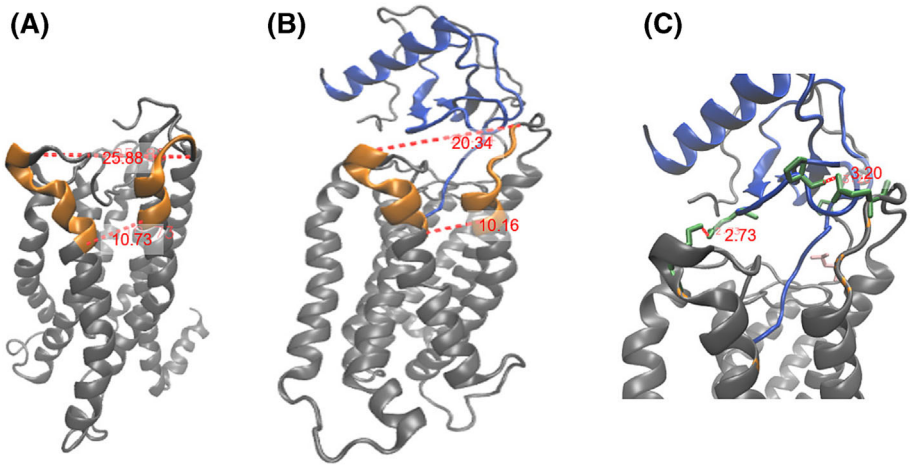

FIGURE 1 Distance of N- and C-terminus of CXC-class chemokine receptor 1 (CXCR1)-derived peptide. (A) NMR structure of CXCR1 as reported by Park et al. (PDB-ID: 2LNL).[14] (B) Final snapshot of CXCR1–CXC-class chemokine ligand 8 (CXCL8) complex from 11-μs molecular dynamics simulation, started from reported atomistic model of CXCL8 bound to CXCR1.[13] CXCR1 is shown in gray. The sequences constituting the IL8RP-Loops peptide (A196-I204 and A264-Q271) are highlighted in orange. The chemokine CXCL8 is depicted in blue. (C) The new contacts of CXCR1-K197 to CXCL8-E29 and CXCR1-Q271 to CXCL8-P32 are shown as dashed lines. Images were created with VMD developed by the Theoretical and Computational Biophysics Group in the Beckman Institute for Advanced Science and Technology at the University of Illinois at Urbana-Champaign (http://www.ks.uiuc.edu/Research/vmd/).[15]

(Saarbrücken, DE), Corning (Kaiserslautern, DE), Ditabis (Pforzheim, DE), Greiner Bio-One International GmbH (Kremsmünster, A), Iris Biotech (Marktredwitz, DE), Macherey & Nagel (Dueren, DE), Merck (Darmstadt, DE), Merck Novabiochem (Darmstadt, DE), Orpegen (Heidelberg, DE), PL-Laboratories (Port Moody, CAN), Rapp Polymers (Tuebingen, DE), Roche (Grenzach-Whylen, DE), Roth (Karlsruhe, DE), TH Geyer (Renningen, DE), Sarstedt (Nümbrecht, DE), Sigma Aldrich (Taufkirchen, DE), Tecan (Maennedorf, CH), and VWR (Darmstadt, DE). Organic solvents in high-performance liquid chromatography (HPLC) purity and for the synthesis of peptides were purchased from VWR. Amino acids conjugated with protection groups as well as primary amines and protection group derivatives were procured from Carbolution and Sigma Aldrich, and coupling reagents for peptide synthesis from Iris Biotech, TH Geyer, Carbolution, and Orpegen. CXCL8 was expressed as described previously (see Supporting Information S1).[13]

2.1 | Molecular dynamics (MD) simulation

2.1.1 | MD simulation and analysis of the CXCR1: CXCL8 complex

A fully atomistic MD system of the previously published CXCR1: CXCL8 complex[13] embedded in a POPC membrane (87 Å × 87 Å) was constructed using CHARMM-GUI.[25] The system was solvated with TIP3P water molecules above and below the membrane, and a total concentration of 0.15 M K^+Cl^- was added with ratio of positive/negative ions adjusted accordingly (automatically during CHARMM-GUI setup) in order to obtain net zero system charge. The MD simulation was performed using the CHARMM36 force field[26] with ACEMD software[27] on specialized GPU-computer hardware. CHARMM provides specialized lipid parameters and is frequently used for MD simulations of GPCRs.[28–30] Briefly, the complex was equilibrated for 20 ns at 300 K (Langevin thermostat) and 1 atm (Berendsen barostat) using a 4-fs time step and electrostatics cut-off of 9.0 Å. During the initial 8 ns of equilibration, harmonic restraints were applied to the protein complex and progressively relaxed over 2-ns steps. During the final 12 ns of equilibration, no restraints were applied. The system was then subjected to a production run of 11 μs without restraints under the same conditions. Analysis of the MD trajectory was made using VMD software[15] v1.9.3 to calculate root mean square deviation (RMSD) of Cα atoms of CXCL8 and CXCR1, and protein–protein interaction potential energies were estimated with the NAMD-energy plugin[31] using default parameters and a dielectric constant of 4.0.

2.1.2 | MD simulation setup of linear and cyclic peptides

All MD simulations were performed using the GROMACS software package (version 2018).[32] For water molecules, we used the SPC/E model,[33] and the peptide interacts through the GROMOS 54A7 force field,[34] as it provides for parameterization of unusual peptide groups and modified amino acids in aqueous environment. The fluorophore (5-carboxy-tetramethylrhodamine [TAMRA]) was modeled via Avogadro[35] and also interacts through the GROMOS 54A7 force field. Charges for the fluorophore were taken from Kyrychenko.[36] The systems were first energy minimized and equilibrated for 2 ns in the NVT-Ensemble at a temperature of 300 K and for 10 ns in the NPT-Ensemble at a temperature of 300 K and a pressure of 1 bar. During the equilibration, temperature was controlled using the velocity-rescale thermostat ($\tau_T = 0.1$ ps),[37] and pressure was controlled using the Berendsen barostat ($\tau_P = 0.5$ ps).[38] Isothermal compressibility was set to 4.5×10^{-5} bar^{-1}. The starting structures were assembled with Avogadro,[35] and a 100-ns simulation was performed to obtain the starting structures. Production runs were performed for 500 ns. The temperature was controlled using the Nosé–Hoover thermostat ($\tau_T = 1$ ps),[39,40] and pressure was controlled using the Parrinello–Rahman barostat ($\tau_P = 1$ ps).[41] Bond lengths were constrained using the LINCS algorithm.[42] A single cut-off of 1.4 nm was used for van-der-Waals interactions. The PME algorithm was used for electrostatic interactions with a cut-off of 1.4 nm. Long range corrections to energy and pressure due to the truncation of Lennard–Jones potential were accounted for. The equations of motion were integrated with a time step of 2 fs.

2.1.3 | Analysis of MD simulation data

In order to analyze structural fluctuations, we used the root mean square fluctuation (RMSF). The RMSF is defined as

$$RMSF(i) = \sqrt{\frac{1}{T}\sum_{t=1}^{T}\left(x_i(t) - x_{ref,i}\right)^2}, \quad (1)$$

where T is the simulation time, $x_i(t)$ the position of particle i at time t, and $x_{ref,i}$ the position of the reference structure of particle i. All RMSF values were calculated with the Biotite package.[43] In order to quantify structural differences and conformational changes for the overall structure of the peptides, we used the RMSD. The RMSD is defined as

$$RMSD(t_1, t_2) = \sqrt{\frac{1}{n}\sum_{i=1}^{n}\left(x_i(t_1) - x_i(t_2)\right)^2}, \quad (2)$$

where n is the number of atoms, $x_i(t_1)$ is the position of particle i at time t_1, and $x_i(t_2)$ is the position of particle i at time t_2. Here, we computed the RMSD between the initial structure ($t_2 = 0$) in all simulations and all simulation frames. The RMSD was calculated with the Biotite package.[43]

Boxplots

The lower end of the box is the 25th percentile, and the upper end of the box is the 75th percentile. The band inside the box is the median. The whiskers are the lowest value still within 1.5 interquartile range

of the lower quartile and the highest value still within 1.5 interquartile range of the upper quartile.

2.2 | Peptide synthesis and purification

2.2.1 | Synthesis of cyclic peptides

Linear precursors of peptides CycloopsE and CycloopsQ were synthesized on AmphiSpheres 40 RAM resin (Agilent Technologies, Santa Clara, CA, USA) with a resin loading capacity of 0.37 mmol g^{-1}. The resin was swollen in dichloromethane (DCM), and the first two amino acids Fmoc-Lys (Mtt)-OH with a 4-methyltrityl (Mtt) side-chain protecting group and Fmoc-Lys (Alloc)-OH with an allyloxycarbonyl (Alloc) side-chain protecting group were coupled manually. For subsequent coupling steps, a standard Fmoc/tBu SPPS protocol was used on a peptide synthesizer (LibertyBlue, CEM, USA) equipped with microwave reactor (Discover, CEM, USA). In this process, 3 eq. Fmoc-protected amino acids were added as a 0.2 M solution in dimethylformamide (DMF). Amino acids were activated by addition of 5 eq. Oxyma and 5 eq. diisopropylcarbodiimide. The Fmoc-protecting group was removed with 20 vol% piperidine and 0.1 M Oxyma in DMF.

Prior to Fmoc deprotection of the N-terminus, the C-terminal lysine residue was selectively deprotected by adding a solution of 1% trifluoroacetic acid (TFA) and 5% triisopropylsilane in DCM and shaking for 5 min to remove the Mtt-protecting group. This procedure was repeated seven times, and the resin was washed three times with 2 mL DCM and three times with 2 mL DMF. Deprotection was monitored with the chloranil test. For labeling the peptides, 3 eq. of 5(6)-carboxy-TAMRA, 3 eq. of 2-(1*H*-benzotriazol-1-yl)-1,1,3,3-tetramethyluronium hexafluorophosphate (HBTU), and 6 eq. of *N*,*N*-diisopropylethylamine (DIPEA) in DMF were added to the resin and shaken for 2 h at room temperature. The resin was washed six times with 2 mL DMF.

For cyclization, the peptide N-terminus was deprotected with 20 vol% piperidine in DMF. The 3 eq. of succinic acid, 3 eq. of HBTU, and 6 eq. of DIPEA in DMF were added to the resin and shaken for 2 h at 600 rpm. For the selective deprotection of the Alloc-protecting group, 3 eq. of tetrakis (triphenylphosphine) palladium(0) were dissolved in a mixture of chloroform, acetic acid, and *N*-methylmorpholine (37:2:1, v:v:v) under N_2 atmosphere. Fifteen milliliters of this solution were added per gram of resin and shaken for 3 h at 600 rpm. The resin was washed alternately with 0.5 vol% DIPEA in DMF and 0.5% sodium diethyldithiocarbamate in DMF until the wash solution remained colorless and six times with 2 mL DMF. For cyclization, 3 eq. of HBTU and 6 eq. of DIPEA in DMF were added, and the mixture was shaken for 5 h. After washing six times with DMF, cyclization was initiated by incubating the resin in a 1% TFA solution in DCM overnight. The supernatant was collected and after cleavage from the solid support pooled with the cleavage supernatant for further use. Completion of cyclization and amine deprotection were monitored with the chloranil test.

2.2.2 | Synthesis of linear peptides

Linear peptides LinloopsE and LinloopsQ were synthesized on Fmoc-Rink Amide AM Polystyrene Resin (Iris BIOTECH GmbH) with a resin loading capacity of 0.59 mmol g^{-1}. The resin was swollen in DCM, and the amino acids were coupled manually using a standard Fmoc/tBu SPPS protocol on an orbital shaker. The Fmoc-protecting groups were removed with 20 vol% piperidine in DMF for 5 and 20 min. Coupling of amino acids was carried out twice for 1 h by using 3 eq. of Fmoc-protected amino acid activated with 3 eq. HBTU and 6 eq. DIPEA. Washing steps were performed with DMF. 5(6)-Carboxy-TAMRA was manually coupled to the N-terminus of the linear peptides after Fmoc deprotection. A solution of 2 eq. of 5(6)-carboxy-TAMRA, 2 eq. of HBTU, and 4 eq. of DIPEA was added to the resin and shaken overnight at ambient temperature. The resin was washed three times with 2 mL DMF, three times with 3 mL of 20 vol% piperidine in DMF, and six times with 2 mL of DMF.

2.2.3 | Determination of resin loading by Fmoc cleavage

Approximately 3–5 mg of resin containing the first Fmoc-protected amino acid were washed with DCM and methanol and dried in vacuo. Beads were weighed and incubated for 30 min in 200 µL of a solution of 2 vol% 1,8-diazabicyclo[5.4.0]undec-7-ene in DMF. Three hundred microliters of acetonitrile were added, and after mixing, 25 µL were transferred to a microfuge tube containing 475 µL of acetonitrile. One hundred microliters of this solution were diluted in 1.15 mL of acetonitrile, and absorption was measured at 304 nm against a blank solution prepared by the same procedure without resin. A correction factor of 16.4 according to Gude et al.[44] was calculated from the molar extinction coefficient of dibenzofulvene in 1,8-diazabicyclo [5.4.0]undec-7-ene/acetonitrile at 304 nm (7624 M^{-1} cm^{-1}) and the dilution factor. The resin loading capacity was calculated by Equation (3):

$$loading\ capacity = \frac{A_{304\,nm} * 16.4}{m_{beads}[mg]} \left[\frac{mmol}{g}\right]. \quad (3)$$

2.2.4 | Chloranil test for free amino groups

A few beads of the synthesis resin were transferred into a microcentrifuge tube. Forty microliters of a 2% chloranil solution in DMF and 40 µL of a 2% acetaldehyde solution in DMF were added. Blue staining of the particles after approximately 5 min indicated the presence of free amino groups.

2.2.5 | Removal of side-chain protecting groups and cleavage from the solid support

For removal of side-chain protecting groups and cleavage of peptides from the polymeric support, a solution of 88% TFA, 5% dithiothreitol, 2% water, 2.5% anisole, and 2.5% triisopropylsilane was prepared. Ten milliliters of this solution were added per gram of resin and shaken for a maximum of 2 h (600 rpm) at ambient temperature. The resin was washed with TFA, and the combined solutions were added to a 10-fold volume of ice-cold methyl-*tert*-butyl ether. The solutions were mixed thoroughly and cooled with liquid nitrogen. Precipitated peptides were centrifuged and washed once with cold methyl-*tert*-butyl ether, and the supernatants were discarded. The precipitates were dissolved in 2 mL of a solution of 50% acetonitrile in water and lyophilized.

2.2.6 | Peptide purification

Peptides were purified by C18 reversed-phase HPLC on a Shimadzu LC20-AD system equipped with two pumps, SPD-M20A photodiode array detector, and 250 × 10 mm Discovery HS C18 RP column (Supelco, Sigma Aldrich) (Table 1). Solution of crude peptide in eluent A (95% water, 5% acetonitrile, and 0.1% TFA) was injected onto the column through a 2-mL injection loop. After washing with 1 column volume (CV) of eluent A, eluent B (5% water, 95% acetonitrile, and 0.1% TFA) concentration was steadily increased from 0% to 75% over 5 CV at a flow rate of 2 mL min^{-1}. Absorption was monitored at 280 and 550 nm for TAMRA-labeled peptides. Fractions were collected and lyophilized manually.

2.3 | Peptide characterization

2.3.1 | Binding experiments

Binding experiments with the cyclic peptides were set up according to an adjusted protocol by Moerke.[45] Sixty-three microliters of a 1 mg mL^{-1} solution of CXCL8 in buffer C (40 mM Na_2HPO_4, 35 mM NaCl, and pH 7.4) was prepared, and 14 consecutive 1:2 dilutions in buffer C were produced by transferring 31.5 µL of solution from one microfuge tube to another containing 31.5 µL of buffer C. The 3.5 µL of 2-µM fluorescently labeled peptide solution were added to every microfuge tube to give a final volume of 35 µL. Additionally, a negative control of peptide without CXCL8 and a blank with plain buffer were prepared. After gentle mixing and centrifugation in a microcentrifuge, 10-µL triplicates of every solution were transferred to adjacent cavities of a 384-well low-volume black wall, transparent flat-bottom microtiter plate (Corning, Kaiserslautern, DE). Samples were measured on a Tecan Infinite M1000 microtiter plate reader (Tecan, Switzerland). For fluorescence intensity, the excitation wavelength was set to 545 nm and the emission wavelength to 579 nm. Fluorescence anisotropy was measured at 530 nm for excitation and 579 nm for emission. For the linear peptides, the highest final concentration of CXCL8 was 60 µM, and the final peptide concentration was 350 nM.

Binding data were evaluated by nonlinear regression in SigmaPlot (Version 12.0; Systat Software, Inc.) by fitting to the sigmoidal dose–response curve with variable slope, *n*:

$$y = \min + \frac{(\max - \min)}{1 + \left(\frac{[CXCL8]}{K_D}\right)^{-n}} = \min + \frac{(max - min) * [CXCL8]^n}{K_D^n + [CXCL8]^n}. \quad (4)$$

Max and min are the maximum and minimum fluorescence intensity or fluorescence anisotropy values, *y* is the measured fluorescence intensity or fluorescence anisotropy, and *n* is the Hill slope. Best fits were obtained with $n = 2$ for fluorescence intensity data and $n = -2$ for fluorescence anisotropy data of the cyclic peptides (inverted curve shape) and $n = 2$ for the linear peptides.

2.3.2 | Protease resistance test

Protease stability was tested by comparing the degradation of fluorescently labeled cyclic and linear peptides in a concentrated trypsin solution. Fifty microliters of a 25-µM peptide solution in buffer C was added to 50 µL of a 1.25-µU solution of trypsin and incubated

TABLE 1 Peptides synthesized in this work with retention time and mass.

Peptide	Sequence	t_R (min)	M (g/mol)
TMR-CycloopsE	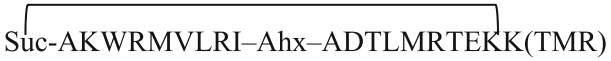	29.8	2950.8
TMR-CycloopsQ	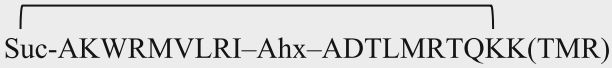	30.0	2949.8
TMR-LinloopsE	TMR-AKWRMVLRI–Ahx–ADTLMRTE	35.9	2615.3
TMR-LinloopsQ	TMR-AKWRMVLRI–Ahx–ADTLMRTQ	36.0	2614.4
LinloopsE	AKWRMVLRI–Ahx–ADTLMRTE	29.0	2202.1
LinloopsQ	AKWRMVLRI–Ahx–ADTLMRTQ	30.0	2201.2

Abbreviations: Ahx, aminohexanoic acid; Suc, succinic acid; TMR, tetramethylrhodamine.

overnight at 37°C and 600 rpm. Afterward, 50 µL of TFA were added to precipitate the enzyme. The solution was centrifuged for 3 min at 2500 × *g*, and a 100-µL sample of the supernatant was analyzed by RP18 HPLC in a linear gradient from 0% to 100% eluent B over 6 CV at a flow rate of 0.4 mL min^{-1}. HPLC was carried out at a Shimadzu LC20-AD system equipped with two pumps, SPD-M20A photodiode array detector, and RP18 column (100 × 2.1 mm, 5-µm Discovery HS C18 RP Supelco, Sigma Aldrich). The TAMRA-labeled peptides were detected at 550 nm; unlabeled peptides were detected at 280 nm. The retention time was 18.5 min for TAMRA-labeled cyclic peptides, 20.1 min for TAMRA-labeled linear peptides, and 19.7 min for unlabeled peptides. A reference sample without trypsin was prepared as described above for every peptide. The area under the curve of the peptide peaks was compared to estimate the amount of intact peptide and thus a measure of protease stability.

2.3.3 | Circular dichroism (CD) spectroscopy

CD spectra were measured in 250 µL of a 25-µM peptide solution in buffer C with a Jasco J-710 at 23°C in 0.1-cm fused silica cuvettes between 200 and 260 nm. The scan interval was kept at 1 nm at a rate of 100 nm min^{-1} with 10 scans per measurement.

3 | RESULTS AND DISCUSSION

3.1 | Design and synthesis of cyclic peptides

To develop an appropriate cyclization strategy for the CXCR1-derived peptides, we considered the distance between Ala196 that corresponds to the peptides' N-terminus and Q271 that forms the C-terminus of IL8RP-LoopsQ to be key. In the reported NMR structure (PDB: 2LNL),[14] the Cα-atoms of these residues are separated by 25.9 Å (see Figure 1A). The previously reported computer-generated full-length atomistic model of the CXCR1:CXCL8 complex[13] was subjected to an unbiased MD simulation of 11 µs. During this MD simulation, several new contacts are formed between CXCL8 and CXCR1 as the complex changes conformation to obtain an energetically more stable interaction (Figure S1). These include the N-terminus of CXCL8 making an electrostatic interaction with E118, located in the core of CXCR1 on transmembrane (TM) helix 3, and the flexible N-terminus of the receptor wrapping around CXCL8 (Figure 1). Of special interest, TM5 and TM6 of CXCR1 also move closer together.

This reduces the distance between amino acids selected as N- and C-terminus of the IL8RP-Loops peptide ([A196-I204]-Ahx-[A264-Q271] by 5.54 Å, and the distance between transmembrane residues I204 and A264 is also reduced by 0.57 Å (see Figure 1B). In the process, a new electrostatic interaction is formed between K197 in CXCR1 (located on ECL2) and E29 of CXCL8 (ε-amine-N-carboxylate-C distance: 3.5 Å) that also interacts with R199 as previously reported.[46] Additionally, a new H-bond between the side chain of Q271 in CXCR1 (located on ECL3; facing outward in the original NMR structure but pointing inward in the MD simulated complex) and the backbone carbonyl group of P32 in CXCL8 (amine-N-carbonyl-C distance: 3.2 Å; see Figure 1C) was observed. Our MD simulated complex differs from the ones published by Liou et al.[47] that were also based on the NMR structure by Park et al.[14] but which used a bovine rhodopsin crystal structure to homology model the N-terminus of CXCR1. In that work, rigid docking was used to propose different binding poses of CXCL8, which led to a final binding pose with the α-helix contacting the receptor and the N-terminus of the chemokine residing on the receptor surface.[47] This is in contradiction with the more recently determined crystal structure of CXCR4 bound to a viral chemokine (PDB id: 4RWS)[48] and subsequent model of the CXCR4:CXCL12 interaction proposed by Wescot et al.[49] in which the chemokine N-terminus is inserted into the opening formed by the ECLs and the transmembrane helices of the receptor. A similar pose was proposed by our MD simulation for CXCR1 and CXCL8 that belongs to the same chemokine class and can therefore be considered plausible.

To allow for equivalent interactions between CXCL8 and a macrocyclic receptor-derived peptide, a linker was needed between the N- and C-terminus, as direct head-to-tail cyclization would bring the N- and C-terminal residues too close together (d = 3.8 Å). Based on a recently published strategy by Chandra et al., we decided to add an additional C-terminal lysine residue and to create a succinimide moiety at the N-terminus for side-chain-to-tail cyclization.[50] The peptide sequence contains an additional lysine that needed to remain protected during cyclization to avoid side reaction. Therefore, Alloc-protected lysine was introduced at the C-terminus that could be removed while leaving the Boc-protecting group on Lys2 intact. In order to monitor binding by fluorescence spectroscopy, we added another lysine at the C-terminus that was immediately deprotected and functionalized with 5(6)-carboxy-TAMRA in a procedure recently described for fluorescein[51] and adopted by us to label cyclic peptoids.[52] TAMRA is less prone to side reactions and more photostable than carboxyfluorescein.[53] It does not change its spectroscopic properties over a wide pH range and does not interact with CXCL8 as we observed previously.[52]

After the synthesis of the peptide sequence, succinic acid was coupled to the N-terminus affording a succinimide moiety. The Alloc group was removed and cyclization proceeded under mild acidic conditions on-resin. An on-bead chloranil test confirmed that all primary amines had reacted during incubation overnight. The peptide was then deprotected and cleaved off the resin under strong acidic conditions (see Scheme 1 for details). As opposed to the report by Chandra,[50] cyclization is possible under mild acidic conditions. Our variant bears the advantage that protecting groups are removed only after cyclization so that lysines and other residues with reactive side chains may be incorporated into the peptide sequence without causing side reactions. The additional lysine at the C-terminus and the N-terminal succinic acid adds up to a total linker length of max. 17.7 Å permitting sufficient flexibility to the former N- and C-terminal peptide residues to interact with remote residues on CXCL8.

We synthesized two cyclic peptides based on the sequence of the previously described receptor-derived peptides: IL8RP-LoopsQ

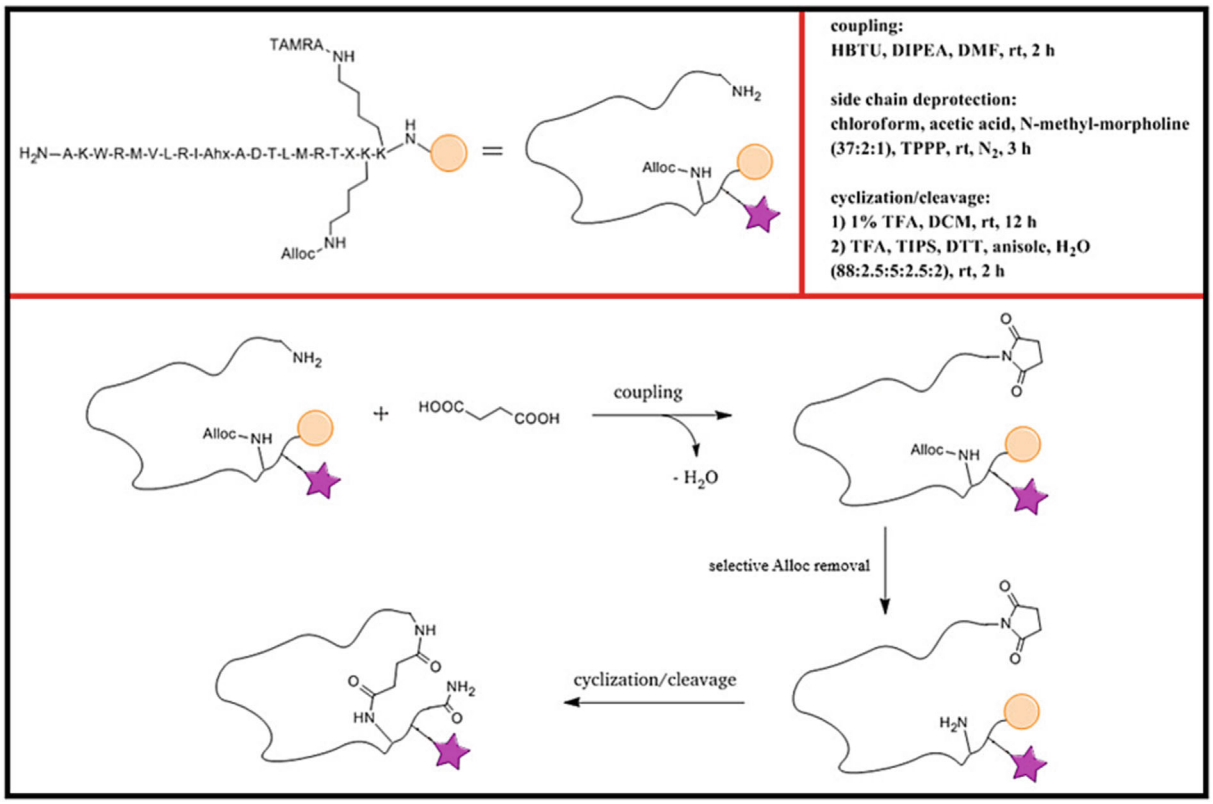

SCHEME 1 Synthesis of TAMRA-labeled peptide macrocycles. After coupling of a first Alloc-lysine to RAM resin (orange sphere) and modification of the deprotected side chain with 5(6)-carboxy-TAMRA (pink star), a second Alloc-lysine is coupled, and the full peptide sequence is synthesized under standard Fmoc conditions. Succinic acid is coupled to the N-terminus yielding a succinimide moiety, the Alloc group is selectively removed, and the lysine side chain reacts with the succinimide under mild acidic conditions. Finally, permanent protecting groups are removed, and the peptide macrocycle is cleaved off the resin. DCM, dichloromethane; DIPEA, *N*,*N*-diisopropylethylamine; DMF, dimethyl formamide; DTT, dithiothreitol; HBTU, 2-(1*H*-benzotriazol-1-yl)-1,1,3,3-tetramethyluronium hexafluorophosphate; rt, room temperature; TAMRA, tetramethylrhodamine; TFA, trifluoroacetic acid; TIPS, triisopropylsilane; TPPP, tetrakis(triphenylphosphine) palladium(0).

corresponded to the original sequence of the CXCR1 ECDs and TMs but showed no affinity in fluorescence polarization experiments[16]; in IL8RP-LoopsE, the C-terminal glutamine was replaced with glutamic acid and an affinity of 2 μM had been measured by fluorescence polarization.[16] With reference to the linear peptides, the new cyclic derivatives were named TMR-CycloopsQ and TMR-CycloopsE. TMR indicates the 5(6)-carboxy-tetramethyl rhodamine label.

3.2 | Binding properties of cyclic peptides

The affinity of the peptide macrocycles to CXCL8 was determined by fluorescence intensity and fluorescence anisotropy measurements. For TMR-CycloopsE, we observed a 3.5-fold increase in fluorescence intensity indicating a change of the chemical environment of the TAMRA label due to interaction with the protein. To our surprise, a fourfold increase in fluorescence intensity was observed for the control peptide TMR-CycloopsQ (Figure 2). Both binding isotherms were best fitted with a Hill slope of 2 indicating the involvement of two molecules of CXCL8. This is in agreement with the dimerization of CXCL8 in the low micromolar concentration range.[54–56] Evaluation of the binding isotherms yielded a K_D of 0.61 ± 0.12 μM for TMR-CycloopsE and 0.99 ± 0.15 μM for TMR-CycloopsQ.

The increase in fluorescence intensity upon the displacement of a fluorophore from a protein is commonly exploited in biosensor systems. Ueda et al. have introduced TAMRA-based biosensors called "quenchbodies" or "Q-bodies" in which the dye is incorporated into single-chain variable region antibody fragments.[57,58] Upon antigen binding to Q-bodies, fluorescence intensity of TAMRA increases as the fluorophore is displaced by the antigen. This displacement upon target binding to the Q-body was demonstrated in a subsequent study using fluorescence anisotropy as a measure of fluorophore mobility.[59]

Fluorescence anisotropy measurements with both of our TAMRA-labeled cyclic peptides revealed inverted binding isotherms with unusually high anisotropy at low protein concentrations and decreasing anisotropy for increasing protein concentrations (see Figure 3). We have observed a similar phenomenon for TAMRA-labeled cyclic peptoids, albeit with lower initial anisotropy values.[52] From these previous measurements and control experiments, we know that TAMRA neither binds to CXCL8 nor to the microtiter plate.[52]

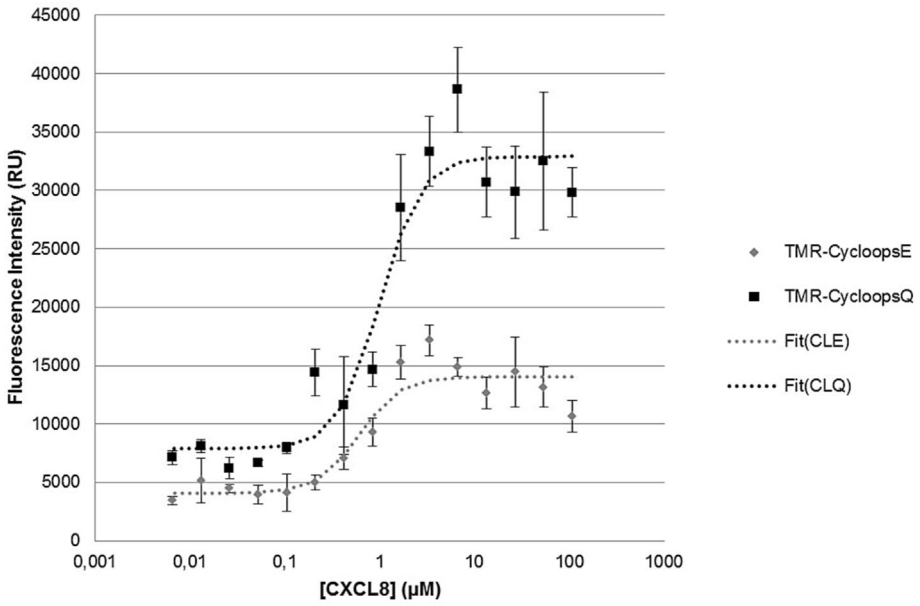

FIGURE 2 Fluorescence intensity measurements for TMR-CycloopsE (gray diamonds) and TMR-CycloopsQ (black squares). Data were fitted in SigmaPlot with sigmoidal dose–response curve with Hill slope $n = 2$ (dashed lines). Error bars represent standard deviation from triplicate measurements. CXCL8, CXC-class chemokine ligand 8.

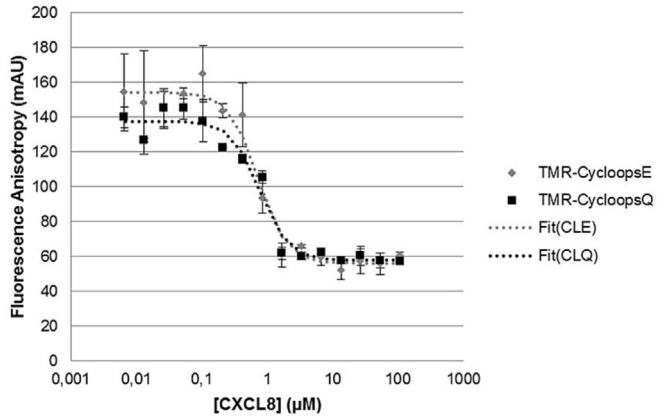

FIGURE 3 Fluorescence anisotropy measurements of cyclic peptides. Gray diamonds: TMR-CycloopsE; black squares: TMR-CycloopsQ. Data were fitted in SigmaPlot with sigmoidal dose–response curve with Hill slope $n = -2$ (dashed lines). Error bars represent standard deviation from triplicate measurements. CXCL8, CXC-class chemokine ligand 8.

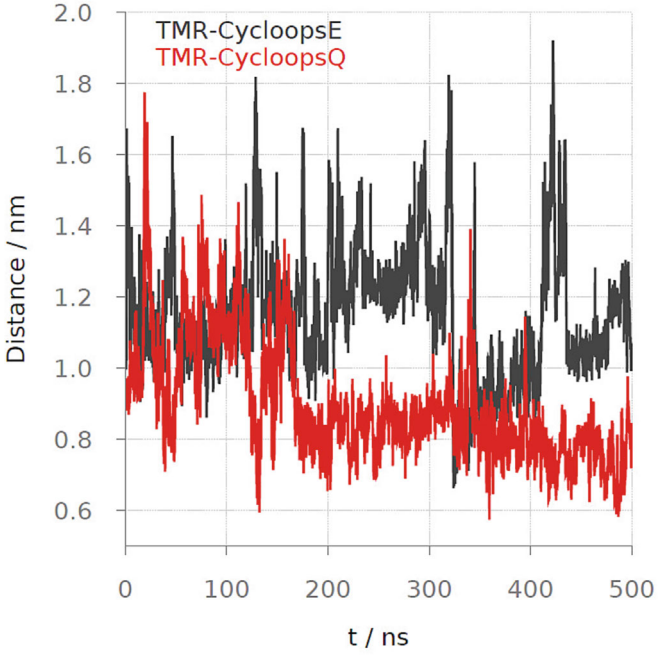

FIGURE 4 Distance between centers of mass of tetramethylrhodamine and the peptide macrocycle over the course of the molecular dynamics simulation. Gray: TMR-CycloopsE; red: TMR-CycloopsQ.

In our cyclic peptides, TAMRA is attached to a flexible linker, that is, the side chain of an exocyclic lysine residue, so that an interaction with the peptide macrocycle is possible. This would lead to high fluorescence anisotropy. The same flexible linker would permit the fluorophore to rotate freely upon displacement leading to low fluorescence anisotropy similar to the free fluorophore. This effect is commonly known as the "propeller effect."[45]

To further support the hypothesis of TAMRA interacting with cyclic peptides, we conducted MD simulations for both peptide macrocycles. By computing the distance between the center of mass (COM) of TAMRA and of the remaining peptide as a function of time, we observed that TAMRA resides in close proximity to the peptide COM. After 200 ns of simulation time, this was more pronounced for TMR-CycloopsQ than for TMR-CycloopsE (see Figure 4).

To identify the position of the fluorophore, we computed the distance between the COM of TAMRA and of each amino acid of the peptide sequence (see Figure 5). We found that TAMRA is in close proximity to the former C-terminal residues M15 to E/Q18 as well as to A1 and K2, which are closer to the attachment point of the label due to cyclization. The distribution of COM distances for TMR-CycloopsQ is narrower than for TMR-CycloopsE and the fluorophore

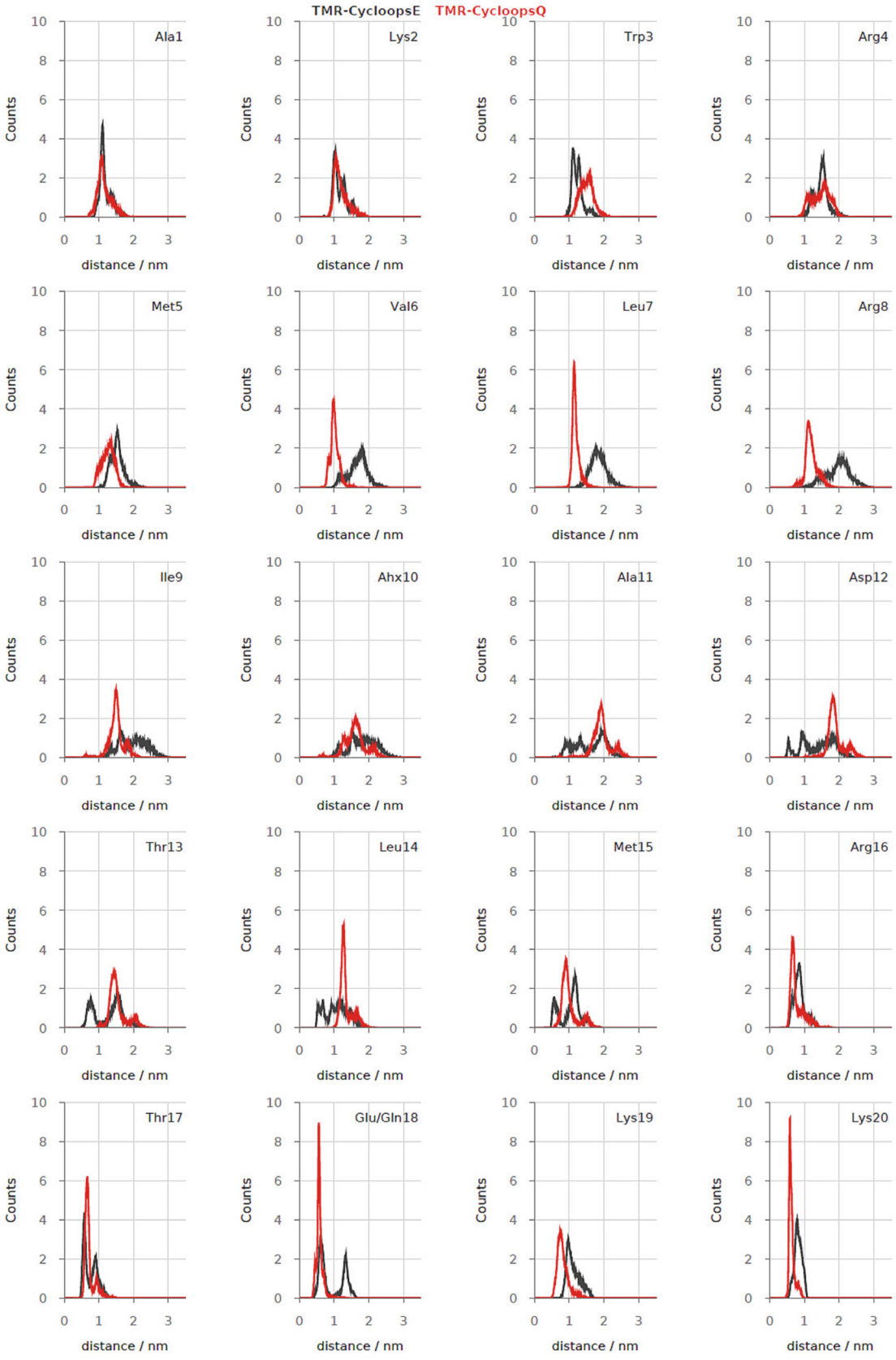

FIGURE 5 Distance of center of mass of tetramethylrhodamine label and center of mass of each individual amino acid of the peptides. Gray: TMR-CycloopsE; red: TMR-CycloopsQ.

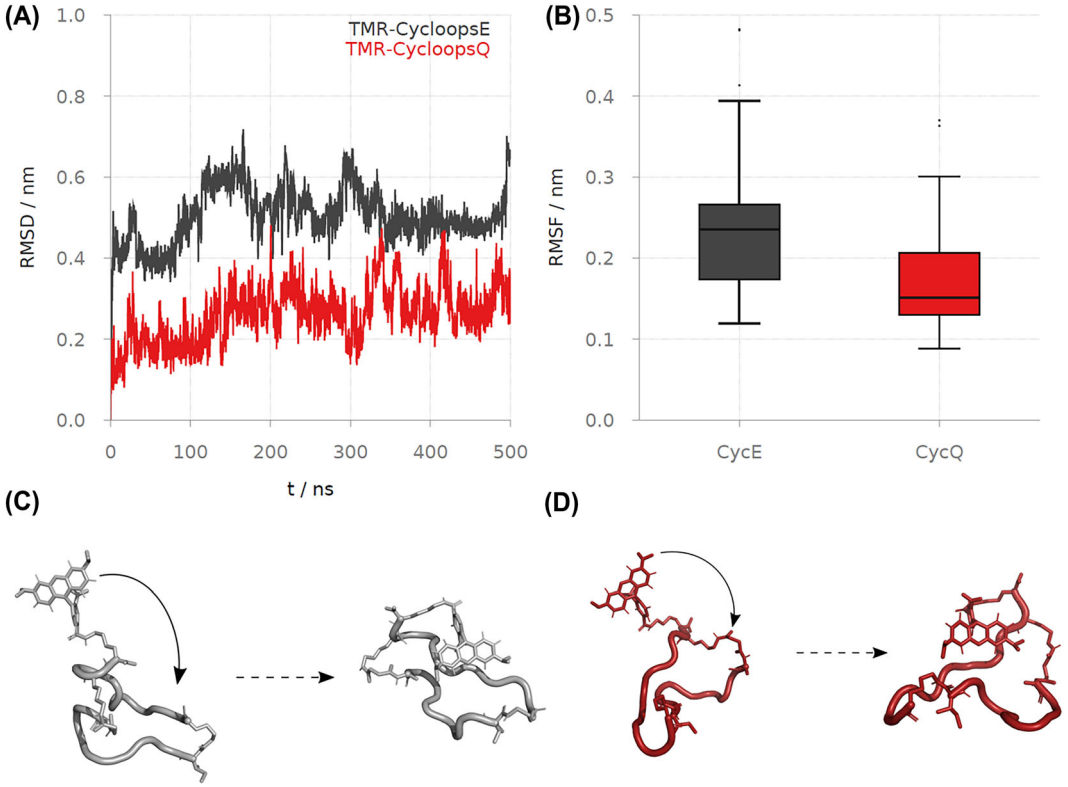

FIGURE 6 Evaluation of molecular dynamics simulations for the TMR-Cycloops peptides. (A) RMSD (top, left) plotted against time and (B) RMSF (top, right) for both peptides. Gray: TMR-CycloopsE; red: TMR-CycloopsQ. Molecular dynamics simulated structures for TMR-CycloopsE (C) and TMR-CycloopsQ (D). Boxplot shows median values and interval between 25th and 75th percentiles (box). Whiskers indicate the 1.5 interquartile range. RMSD, root mean square deviation; RMSF, root mean square fluctuation.

also seems to approach residues V6, L7, and R8 in TMR-CycloopsQ, bridging opposite sides of the peptide macrocycle.

Additionally, we compared RMSD values for both compounds as a function of time. Both peptides slightly change their conformation (see Figure 6A) but the RMSD of TMR-CycloopsQ is generally lower, which is in agreement with its smaller distances and narrower distribution between relevant COMs compared with TMR-CycloopsE (Figures 4 and 5). In support of this, an evaluation of the RMSF shows that TMR-CycloopsQ assumes a more rigid structure than TMR-CycloopsE (see Figure 6B). However, over the course of their respective MD simulations, both peptides adopt a general conformation in which the fluorophore resides in close proximity to the peptide macrocycle (see Figure 6C,D).

The Ueda group attributed the low fluorescence intensity of their Q-bodies in the antigen-free state to quenching of the TAMRA fluorescence by nearby tryptophan residues via photoinduced electron transfer.[57] This explanation should also be valid for the cyclic IL8RP-Loops peptides that contain a tryptophan residue in position 3. The MD simulations show that the COM of TAMRA resides within a distance of 1–2 nm from the COM of Trp3 (see Figure 5) which would be sufficient for electron transfer.[60] The interaction of TAMRA with the peptide macrocycles would account for the low fluorescence intensity and high fluorescence anisotropy values observed for the free peptide and at low chemokine concentrations.

Assuming this model is valid, the fluorophore should also be displaced by nonspecific binders, detergents, or denaturing reagents. We therefore investigated the fluorescence anisotropy of TMR-CycloopsE/Q in the presence of buffer C, after addition of bovine serum albumin and Triton X-100 that are commonly used as inhibitors of nonspecific interactions in binding experiments and in the presence of 8 M guanidinium hydrochloride as a denaturing agent. As shown in Figure 7, none of these additives had an impact on the fluorescence anisotropy of TAMRA, but the fluorescence anisotropy of both TMR-Cycloops peptides was reduced almost to the level of free TAMRA dye. Apparently, all agents are able to disrupt the interaction of TAMRA with the peptide macrocycles.

Due to the increase in fluorescence intensity upon protein binding, fluorescence anisotropy values need to be corrected prior to evaluation. We used the corrections described by Dandliker[61] and by Lundblad[62] that yielded slightly higher K_D values compared with direct evaluation (see Table 2).

For all evaluation modes, K_D values were identical for TMR-CycloopsE and TMRCycloopsQ within experimental error (see Table 1). They were also identical to the affinity of linear IL8RP-LoopsE[13,16] within experimental error. Thus, cyclization seems to have no impact on affinity for the LoopsE sequence, and the affinity of the LoopsQ sequence, for which no affinity had been detected in previous studies,[13,16] exhibits the same affinity as LoopsE. We have also

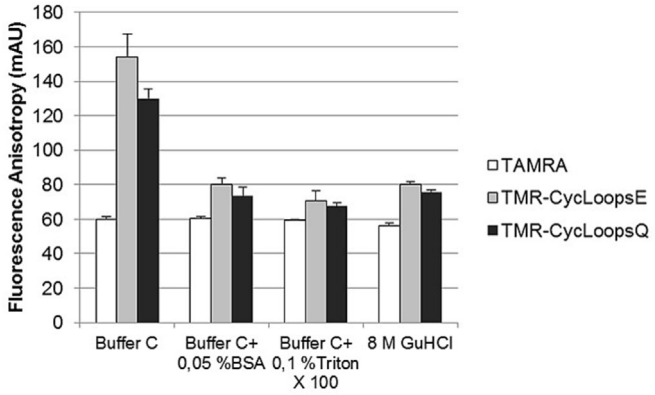

FIGURE 7 Effect of buffer additives on fluorescence anisotropy. Bovine serum albumin (BSA), Triton X-100, and 8 M guanidinium hydrochloride (GuHCl) reduce the fluorescence anisotropy of both TMR-CycloopsE (gray) and TMR-CycloopsQ (black) while having no impact on free TAMRA dye (white). TAMRA, tetramethylrhodamine.

TABLE 2 K_D values of TMR-CycloopsE and TMR-CycloopsQ calculated from different experiments with different methods.

Method	K_D (TMR-CycloopsE) (μM)	K_D (TMR-CycloopsQ) (μM)
Fluorescence intensity	0.61 ± 0.12	0.99 ± 0.15
FA direct evaluation	0.72 ± 0.09	0.77 ± 0.08
FA Dandliker correction[61]	1.15 ± 0.23	1.21 ± 0.21
FA Lundblad correction[62]	1.15 ± 0.23	1.22 ± 0.21

observed different levels of fluorescence anisotropy for free and bound species in the present and previous studies.[52] This could imply that the N-terminal fluorescein label used previously[16] had resulted in equal fluorescence anisotropy values for free and bound peptide. Therefore, we synthesized the linear peptides TMR-LinloopsE and TMR-LinloopsQ with an N-terminal TAMRA label. In binding experiments with CXCL8, fluorescence intensity decreased with increasing CXCL8 concentration (see Figure 8A). Due to the large standard deviations, these data were not suitable for estimating K_D values. Fluorescence anisotropy increased with increasing CXCL8 concentration up to 3.7 μM. At higher CXCL8 concentrations, fluorescence anisotropy decreased almost reaching the value of the free linear peptide (see Figure 8B). Interestingly, fluorescence anisotropy values were almost identical for TMR-LinloopsE and TMR-LinloopsQ, suggesting that the linear peptides interact similarly with CXCL8.

The drop in fluorescence anisotropy at high concentrations could not be attributed to the decrease in intensity as correction according to Dandliker[61] did not result in a plateau at high concentrations. Absorption measurements revealed an increase in absorption at increasing CXCL8 concentrations (see Figure S2a) and absorption spectra showed a strong increase at short wavelengths typical of light scattering (see Figure S2b). These findings suggest that a precipitate forms at high CXCL8 concentrations. Therefore, fluorescence anisotropy values for CXCL8 concentrations >3.7 μM were not included in the evaluation. This way, K_D values of 0.80 ± 0.06 μM for TMR-LinloopsE and 0.71 ± 0.09 μM for TMR-LinloopsQ were obtained. Thus, the affinity of the TAMRA-labeled peptides equals the affinity reported for the fluorescein-labeled LinloopsE[13,16] within experimental error. We assume that, for the fluorescein-labeled LinloopsQ reported earlier,[13,16] fluorescence anisotropy of the free peptide and the protein-bound species were almost equal so that no affinity could be measured by the fluorescence anisotropy experiment. This will need to be confirmed by a label-free binding assay in future studies.

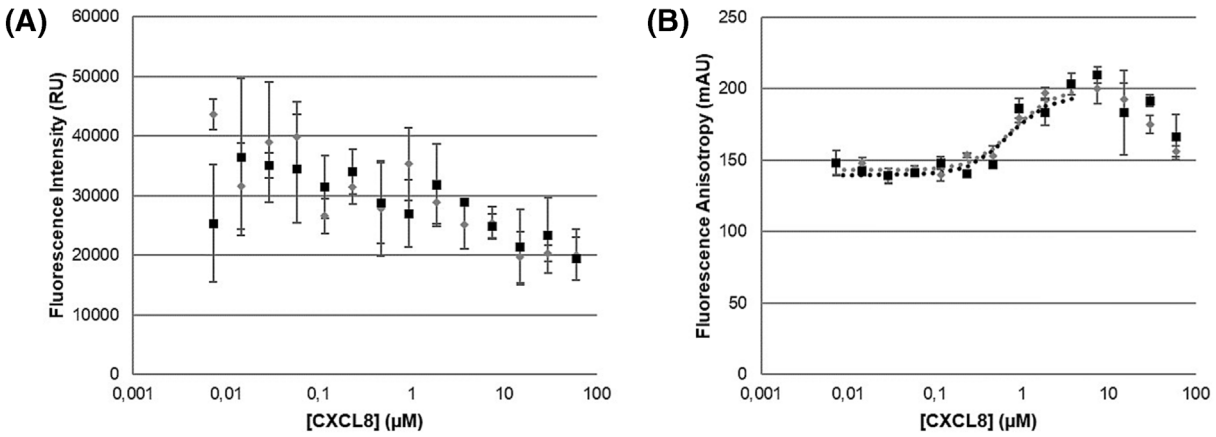

FIGURE 8 Binding characteristics of linear peptides. Gray diamonds: TMR-LinloopsE; black squares: TMR-LinloopsQ. (A) Fluorescence intensity, due to the high standard deviation, data were not fitted. (B) Fluorescence anisotropy measurement. Data were fitted in SigmaPlot with sigmoidal dose–response curve with exponent $n = 2$ (dashed lines) for CXCL8 concentrations up to 3.7 μM. Larger concentrations values were not included in the evaluation due to the observed precipitation. Error bars represent standard deviation from triplicate measurements. CXCL8, CXC-class chemokine ligand 8.

Macrocyclization did not increase affinity. We assume that the large ring size of 18 amino acids combined with the flexible Ahx linker and the long lysine-succinate-linker employed for cyclization leaves the macrocycle sufficiently flexible so that the difference in entropic cost for binding to CXCL8 compared with the linear peptides may be small. Displacement of the fluorophore comes at an enthalpic cost for the overall binding process that could compensate for the potentially small gain in entropy. The impact of the fluorophore on affinity will have to be elucidated in subsequent studies with labeled and unlabeled peptides in a label-free binding assay.

3.3 | Protease stability

The second goal of our macrocyclization project was the stabilization of the IL8RP-Loops peptides against proteases. The interaction of the TAMRA fluorophore with the peptide macrocycle might further impede protease interaction. Interaction with the TAMRA label might also convey some degree of protection against proteases for the linear peptides. We therefore conducted trypsin digestion experiments with the TAMRA-labeled cyclic and linear peptides as well as with the unlabeled linear peptides. TAMRA was coupled to the N-terminus of the linear peptides, and the C-terminal lysines for labeling and macrocyclization were both omitted. The IL8RP-Loops sequence contains one lysine and three arginine residues offering a total of four cleavage sites for trypsin. The area under the HPLC peak representing the intact peptide was compared with the area under the curve for the same retention time interval of the sample after tryptic digestion (see Table 3).

TABLE 3 Peptide loss due to tryptic digestion for differently labeled peptide variants.

Variant	LoopsE (%)	LoopsQ (%)
TAMRA, cyclic	0.26	0.69
TAMRA, linear	12.4	18.4
Unlabeled, linear	50.6	61.3

Abbreviation: TAMRA, tetramethylrhodamine.

After incubation with trypsin overnight, the unlabeled peptides were degraded by 51% (E) and 61% (Q), respectively, and no degradation could be detected for the cyclic peptides. Interestingly, the TAMRA-labeled linear peptides were only degraded by 12% (E) and 18% (Q), suggesting a protective effect of the TAMRA label. In general, the linear derivatives of IL8RP-LoopsE seemed to be somewhat more stable with proteases than the corresponding IL8RP-LoopsQ derivatives. The MD simulations for the cyclic peptides suggest that the LoopsQ sequence is more rigid (see Figures 4 and 6A,B). If this was also true for the linear sequences, this could explain the differences seen in protease stability.

To address both issues, we performed further MD simulations for the TAMRA-labeled and unlabeled linear peptides. Analysis of the distances between the COMs of the peptide and fluorophore reveals that the median distance is similar for linear and cyclic peptides (see Figure 9A). The distribution of distances found over the course of MD simulations was larger for the E variants compared with the respective Q variants, indicating greater flexibility of the former.

In the linear IL8RP-LoopsQ peptide, the fluorophore seems to preferentially reside closer to the hydrophobic residues M6, L8, and Vl7 (see Figure S3). Analysis of the RMSD over the course of the MD simulation of the cyclic and linear peptides shows no correlation with the protease stability test (see Figure S4). As shown in Figure 9B, CD spectra of all six peptides indicate that the Q variants are less structured than the corresponding E variants, which exhibit a strong minimum at 200 nm, indicative of quarternary structure as seen for coiled coils,[63] collagen triple helices,[64] or quadruple helices formed by certain α/β-peptides.[65] The lesser propensity to assume such structures could explain why Q variants are slightly more prone to degradation than the E variants that appear to associate into more ordered structures at the higher concentrations needed for CD spectroscopy.

Apparently, TAMRA-labeled linear peptides are more stable than unlabeled linear peptides, as their N-terminus is protected by the fluorophore and the TAMRA label also hinders protease interaction by spatial proximity to the rest of the peptide chain. In the cyclic peptides, the N-terminus is protected due to head-to-tail macrocyclization and TAMRA residing in proximity to the macrocycle, preventing

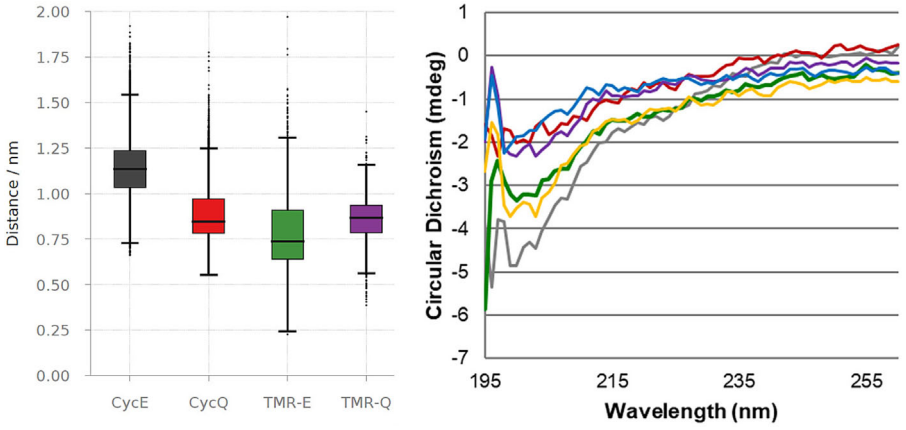

FIGURE 9 Analysis of peptide flexibility. (A) Distances between center of mass of the cyclic or linear peptides and center of mass of the fluorophore. Boxplots show median values and interval between 25th and 75th percentiles (box). Whiskers indicate the 1.5 interquartile range. (B) Circular dichroism spectra of all peptides recorded at 25 µM in buffer C; gray: TMR-CycloopsE, red: TMR-CycloopsQ, green: TMR-LinloopsE, purple: TMR-LinloopsQ, yellow: LinloopsE, and blue: LinloopsQ.

protease interaction and compensating for chain flexibility, making the TMR-Cycloops peptides virtually immune toward trypsin digestion. The tendency of the E variants to associate may explain why they are somewhat more stable against trypsin digestion. This will be subject to further investigation.

4 | CONCLUSIONS AND OUTLOOK

To improve the properties of the CXCR1-derived peptide IL8RP-LoopsE by cyclization, we have performed an MD simulation of the CXCL8–CXCR1 complex to identify a cyclization strategy that leaves functional groups required for interaction with CXCL8 intact. Protected peptides with a TAMRA label on a C-terminal lysine residue were cyclized on-bead via a second C-terminal lysine side chain and an N-terminal linker. Not only the cyclic version of IL8RP-LoopsE was found to bind to CXCL8 but also a cyclic version of the original sequence featuring a C-terminal glutamine, for which no binding had been detected in previous studies. In experiments with linear TAMRA-labeled peptides, both sequences exhibited almost identical binding to CXCL8, partly explaining the similar affinity observed with cyclized peptides. In binding assays with the cyclic TAMRA-labeled peptides, we found an increase of fluorescence intensity and a decrease in fluorescence anisotropy with increasing target protein concentration. These observations could be attributed to an interaction of the fluorophore with the peptide macrocycle that is displaced by interaction with its binding partner, CXCL8. This effect could be exploited in peptide-based biosensors. For this purpose, the interaction of TAMRA and other fluorophores with linear and cyclic peptides of different ring sizes need to be studied systematically. Cyclization of the 18mer IL8RP-Loops peptides had no impact on affinity with CXCL8, which may be due to the large ring size or the free energy costs for displacement of the fluorophore from the peptide macrocycle. This needs to be investigated in future studies using label-free binding assays. To increase affinity, cyclization strategies with more rigid linkers between the two peptide moieties and the insertion of a second covalent bond to form a bicyclic system will be tested. Interestingly, cyclization prevented trypsin digestion, whereas an N-terminal TAMRA label turned out to reduce proteolytic digestion. The described effects may be exploited for biosensor development and peptide stabilization and need to be kept in mind when choosing TAMRA as a fluorophore for peptide labeling.

AUTHOR CONTRIBUTIONS

Conceptualization, K.B., P.B., J.S.W., and K.S.; methodology, K.B., P.B., J.S.W., J.A.R.D., and K.S.; validation, K.B., P.B., J.S.W., J.A.R.D., and K.S.; formal analysis, K.B., P.B., J.S.W., J.A.R.D., and K.S.; investigation, K.B., P.B., J.S.W., J.A.R.D., and K.S.; resources, K.S.; data curation, K.B., P.B., J.S.W., J.A.R.D., and K.S.; writing—original draft preparation, K.B., P.B., J.S.W., J.A.R.D., and K.S.; writing—review and editing, K.B., P.B., J.S.W., J.A.R.D., and K.S.; visualization, K.B., P.B., J.S.W., J.A.R.D., and K.S.; supervision, K.S.

ACKNOWLEDGEMENTS

We thank Heiko Fittler, Sascha Knauer, Hendrik Schneider, and Sebastian Hörner for LC-MS measurements, Dana Schmidt for assistance with peptide synthesis, Anke Imrich for the production of recombinant CXCL8, and Olga Avrutina, Joachim Hönes, and Kay Hamacher for helpful discussions. We thank Alexander Heckel and Christian Grünewald (Goethe University, Frankfurt a.M.) for granting us access to their CD spectrometer and Philipp Czechowski for CD measurements at TU Darmstadt. Open Access funding enabled and organized by Projekt DEAL.

CONFLICT OF INTEREST STATEMENT

The authors declare no conflict of interest.

DATA AVAILABILITY STATEMENT

All measurement data can be made available upon request.

ORCID

Katja Schmitz https://orcid.org/0000-0001-9023-318X

REFERENCES

1. Helmer D, Schmitz K. Peptides and peptide analogs to inhibit protein-protein interactions. *Adv Exp Med Biol*. 2016;(917):147-183. Published online May 30, 2016, doi:10.1007/978-3-319-32805-8_8
2. Wang X, Ni D, Liu Y, Lu S. Rational design of peptide-based inhibitors disrupting protein-protein interactions. *Front Chem*. 2021;9:682675. Published online May 4, 2021, doi:10.3389/fchem.2021.682675
3. Pandey S, Malviya G, Chottova Dvorakova M. Role of peptides in diagnostics. *Int J Mol Sci*. 2021;22(16):8828. Published online August 17, 2021, doi:10.3390/ijms22168828
4. Shpakov AO. Signal protein-derived peptides as functional probes and regulators of intracellular signaling. *J Amino Acids*. 2011;2011:656051. Published online August 23, 2011, doi:10.4061/2011/656051
5. Robinson JA, Demarco S, Gombert F, Moehle K, Obrecht D. The design, structures and therapeutic potential of protein epitope mimetics. *Drug Discov Today*. 2008;13(21-22):944-951. Published online September 11, 2008, doi:10.1016/j.drudis.2008.07.008
6. Bachelerie F, Ben-Baruch A, Burkhardt AM, et al. Zlotnik, A. International Union of Basic and Clinical Pharmacology. [corrected]. LXXXIX. Update on the extended family of chemokine receptors and introducing a new nomenclature for atypical chemokine receptors. *Pharmacol Rev*. 2014;66(1):1-79. Published online November 13, 2013, doi:10.1124/pr.113.007724
7. Szpakowska M, Fievez V, Arumugan K, van Nuland N, Schmit J-C, Chevigné A. Function, diversity and therapeutic potential of the N-terminal domain of human chemokine receptors. *Biochem Pharmacol*. 2012;84(10):1366-1380. doi:10.1016/j.bcp.2012.08.008
8. Rajagopalan L, Rajarathnam K. Structural basis of chemokine receptor function—a model for binding affinity and ligand selectivity. *Biosci Rep*. 2006;26(5):325-339. Published online October 7, 2006, doi:10.1007/s10540-006-9025-9
9. Thiele S, Rosenkilde MM. Interaction of chemokines with their receptors—from initial chemokine binding to receptor activating steps. *Curr Med Chem*. 2014;21(31):3594-3614. doi:10.2174/092986732166140716093155
10. Chevigné A, Fievez V, Szpakowska M, et al. Neutralising properties of peptides derived from CXCR4 extracellular loops towards CXCL12 binding and HIV-1 infection. *Biochim Biophys Acta*. 2014;1843(5):1031-1041. Published online February 1, 2014, doi:10.1016/j.bbamcr.2014.01.017

11. Agrawal L, VanHorn-Ali Z, Berger EA, Alkhatib G. Specific inhibition of HIV-1 coreceptor activity by synthetic peptides corresponding to the predicted extracellular loops of CCR5. *Blood*. 2004;103(4):1211-1217. doi:10.1182/blood-2003-08-2669
12. Möbius K, Dürr R, Haußner C, Dietrich U, Eichler J. A functionally selective synthetic mimic of the HIV-1 co-receptor CXCR4. *Chem – Eur J*. 2012;18(27):8292-8295. doi:10.1002/chem.201200111
13. Helmer D, Rink I, Dalton JAR, et al. Rational design of a peptide capture agent for CXCL8 based on a model of the CXCL8:CXCR1 complex. *RSC Adv*. 2015;5(33):25657-25668. doi:10.1039/C4RA13749C
14. Park SH, Das BB, Casagrande F, et al. Structure of the chemokine receptor CXCR1 in phospholipid bilayers. *Nature*. 2012;491(7426):779-783. doi:10.1038/nature11580
15. Humphrey W, Dalke A, Schulten K. VMD: visual molecular dynamics. *J Mol Graph*. 1996;14(1):33-38. doi:10.1016/0263-7855(96)00018-5
16. Helmer D, Rink I, Dalton JAR, et al. Correction: rational design of a peptide capture agent for CXCL8 based on a model of the CXCL8:CXCR1 complex. *RSC Adv*. 2018;8(30):16800-16801. Published online May 9, 2018. doi:10.1039/c8ra90035c
17. Bodanszky M, Martinez J. Side reactions in peptide synthesis. In: Gross E, Meienhofer J, eds. *The Peptides: Analysis, Synthesis, Biology*. Vol. 5. Academic Press; 1983.
18. Farilie DP, Abbenante G, March DR. Macrocyclic peptidomimetics—forcing peptides into bioactive conformations. *Curr Med Chem*. 1995;2(2):654-686. doi:10.2174/092986730266220218001506
19. Cowell SM, Lee YS, Cain JP, Hruby VJ. Exploring Ramachandran and chi space: conformationally constrained amino acids and peptides in the design of bioactive polypeptide ligands. *Curr Med Chem*. 2004;11(21):2785-2798. doi:10.2174/0929867043364270
20. White CJ, Yudin AK. Contemporary strategies for peptide macrocyclization. *Nat Chem*. 2011;3(7):509-524. doi:10.1038/nchem.1062
21. Cardote TAF, Ciulli A. Cyclic and macrocyclic peptides as chemical tools to recognise protein surfaces and probe protein-protein interactions. *ChemMedChem*. 2016;11(8):787-794. Published online November 13, 2015, doi:10.1002/cmdc.201500450
22. Monroc S, Badosa E, Feliu L, Planas M, Montesinos E, Bardají E. De novo designed cyclic cationic peptides as inhibitors of plant pathogenic bacteria. *Peptides*. 2006;27(11):2567-2574. doi:10.1016/j.peptides.2006.04.019
23. Millward SW, Fiacco S, Austin RJ, Roberts RW. Design of cyclic peptides that bind protein surfaces with antibody-like affinity. *ACS Chem Biol*. 2007;2(9):625-634. doi:10.1021/cb7001126
24. Ahn H, Cho W, Kim J, et al. Design and synthesis of cyclic disulfide-bonded antibacterial peptides on the basis of the α helical domain of Tenecin 1, an insect defensin. *Bioorg Med Chem Lett*. 2008;16(7):4127-4137. doi:10.1016/j.bmc.2008.01.019
25. Jo S, Kim T, Iyer VG, Im W. CHARMM-GUI: a web-based graphical user interface for CHARMM. *J Comput Chem*. 2008;29(11):1859-1865. doi:10.1002/jcc.20945
26. Huang J, MacKerell AD. CHARMM36 all-atom additive protein force field: validation based on comparison to NMR data. *J Comput Chem*. 2013;34(25):2135-2145. Published Online: July 6, 2013. doi:10.1002/jcc.23354
27. Harvey MJ, Giupponi G, de Fabritiis G. ACEMD: accelerating biomolecular dynamics in the microsecond time scale. *J Chem Theory Comput*. 2009;5(6):1632-1639. Published online May 21, 2009, doi:10.1021/ct9000685
28. Bruzzese A, Dalton JAR, Giraldo J. Insights into adenosine A2A receptor activation through cooperative modulation of agonist and allosteric lipid interactions. *PLoS Comput Biol*. 2020;16(4):e1007818. Published online April 16, 2020, doi:10.1371/journal.pcbi.1007818
29. Patra SM, Chakraborty S, Shahane G, et al. Differential dynamics of the serotonin1A receptor in membrane bilayers of varying cholesterol content revealed by all atom molecular dynamics simulation. *Mol Membr Biol*. 2015;32(4):127-137. doi:10.3109/09687688.2015.1096971
30. Cang X, Du Y, Mao Y, Wang Y, Yang H, Jiang H. Mapping the functional binding sites of cholesterol in β2-adrenergic receptor by long-time molecular dynamics simulations. *J Phys Chem B*. 2013;117(4):1085-1094. Published online January 16, 2013, doi:10.1021/jp3118192
31. Phillips JC, Braun R, Wang W, et al. Scalable molecular dynamics with NAMD. *J Comput Chem*. 2005;26(16):1781-1802. Published Online: October 14, 2005. doi:10.1002/jcc.20289
32. Abraham MJ, Murtola T, Schulz R, et al. GROMACS: high performance molecular simulations through multi-level parallelism from laptops to supercomputers. *SoftwareX*. 2015;1-2:19-25. doi:10.1016/j.softx.2015.06.001
33. Berendsen HJC, Grigera JR, Straatsma TP. The missing term in effective pair potentials. *J Phys Chem*. 1987;91(24):6269-6271. doi:10.1021/j100308a038
34. Schmid N, Eichenberger AP, Choutko A, et al. Definition and testing of the GROMOS force-field versions 54A7 and 54B7. *Eur Biophys J*. 2011;40(7):843-856. doi:10.1007/s00249-011-0700-9
35. Hanwell MD, Curtis DE, Lonie DC, Vandermeersch T, Zurek E, Hutchison GR. Avogadro: an advanced semantic chemical editor, visualization, and analysis platform. *J Chem*. 2012;4(1):17. doi:10.1186/1758-2946-4-17
36. Kyrychenko A. A molecular dynamics model of rhodamine-labeled phospholipid incorporated into a lipid bilayer. *Chem Phys Lett*. 2010;485(1):95-99. doi:10.1016/j.cplett.2009.12.015
37. Bussi G, Donadio D, Parrinello M. Canonical sampling through velocity rescaling. *J Chem Phys*. 2007;126(1):14101. doi:10.1063/1.2408420
38. Berendsen HJC, Postma JPM, van Gunsteren WF, DiNola A, Haak JR. Molecular dynamics with coupling to an external bath. *J Chem Phys*. 1984;81(8):3684-3690. doi:10.1063/1.448118
39. Nosé S. A molecular dynamics method for simulations in the canonical ensemble. *Mol Phys*. 1984;52(2):255-268. doi:10.1080/00268978400101201
40. Hoover WG. Canonical dynamics: equilibrium phase-space distributions. *Phys Rev A*. 1985;31(3):1695-1697. doi:10.1103/PhysRevA.31.1695
41. Parrinello M, Rahman A. Polymorphic transitions in single crystals: a new molecular dynamics method. *J Appl Phys*. 1981;52(12):7182-7190. doi:10.1063/1.328693
42. Hess B, Bekker H, Berendsen HJC, Fraaije JGEM. LINCS: a linear constraint solver for molecular simulations. *J Comput Chem*. 1997;18(12):1463-1472. doi:10.1002/(sici)1096-987x(199709)18:12%3C1463:aid-jcc4%3E3.0.co;2-h
43. Kunzmann P, Hamacher K. Biotite: a unifying open source computational biology framework in Python. *BMC Bioinformatics*. 2018;19(1):346. Published online October 1, 2018, doi:10.1186/s12859-018-2367-z
44. Gude M, Ryf J, White PD. An accurate method for the quantitation of Fmoc-derivatized solid phase supports. *Lett Pept Sci*. 2002;9(4):203-206. doi:10.1023/A:1024148619149
45. Moerke NJ. Fluorescence polarization (FP) assays for monitoring peptide-protein or nucleic acid-protein binding. *Curr Protoc Chem Biol*. 2009;1(1):1-15. doi:10.1002/9780470559277.ch090102
46. Leong SR, Kabakoff RC, Hebert CA. Complete mutagenesis of the extracellular domain of interleukin-8 (IL-8) type A receptor identifies charged residues mediating IL-8 binding and signal transduction. *J Biol Chem*. 1994;269(30):19343-19348. Published online July 29, 1994.
47. Liou J-W, Chang F-T, Chung Y, Chen W-Y, Fischer WB, Hsu H-J. In silico analysis reveals sequential interactions and protein conformational changes during the binding of chemokine CXCL-8 to its receptor CXCR1. *PLoS ONE*. 2014;9(4):e94178. doi:10.1371/journal.pone.0094178

48. Qin L, Kufareva I, Holden LG, et al. Structural biology. Crystal structure of the chemokine receptor CXCR4 in complex with a viral chemokine. *Science (New York, NY)*. 2015;347(6226):1117-1122. Published online January 22, 2015, doi:10.1126/science.1261064
49. Wescott MP, Kufareva I, Paes C, et al. Signal transmission through the CXC chemokine receptor 4 (CXCR4) transmembrane helices. *Proc Natl Acad Sci*. USA. 2016;113(35):9928-9933. doi:10.1073/pnas.1601278113
50. Chandra K, Roy TK, Shalev DE, et al. A tandem in situ peptide cyclization through trifluoroacetic acid cleavage. *Angew Chem Int Ed*. 2014;53(36):9450-9455. doi:10.1002/anie.201402789
51. Oh M, Lee JH, Moon H, Hyun Y-J, Lim H-S. A chemical inhibitor of the Skp2/p300 interaction that promotes p53-mediated apoptosis. *Angew Chem Int Ed*. 2016;55(2):602-606. doi:10.1002/anie.201508716
52. Brahm K, Wack JS, Eckes S, Engemann V, Schmitz K. Macrocyclization enhances affinity of chemokine-binding peptoids. *Pept Sci*. 2019;110(4):e23244. Published online December 13, 2018, doi:10.1002/bip.23244
53. Fischer R, Mader O, Jung G, Brock R. Extending the applicability of carboxyfluorescein in solid-phase synthesis. *Bioconjug Chem*. 2003;14(3):653-660. Published online May 22, 2003, doi:10.1021/Bc025658b
54. Burrows SD, Doyle ML, Murphy KP, et al. Determination of the monomer-dimer equilibrium of interleukin-8 reveals it is a monomer at physiological concentrations. *Biochemistry*. 1994;33(43):12741-12745. Published online: November 1, 1994, doi:10.1021/bi00209a002
55. Paolini JF, Willard D, Consler T, Luther M, Krangel MS. The chemokines IL-8, monocyte chemoattractant protein-1, and I-309 are monomers at physiologically relevant concentrations. *J Immunol*. 1994;153(6):2704-2717. doi:10.4049/jimmunol.153.6.2704
56. Lowman HB, Fairbrother WJ, Slagle PH, et al. Monomeric variants of IL-8: effects of side chain substitutions and solution conditions upon dimer formation. *Protein Sci*. 1997;6(3):598-608. Published online March 1, 1997, doi:10.1002/pro.5560060309
57. Abe R, Ohashi H, Iijima I, et al. "Quenchbodies": quench-based antibody probes that show antigen-dependent fluorescence. *J Am Chem Soc*. 2011;133(43):17386-17394. Published online October 6, 2011, doi:10.1021/ja205925j
58. Jeong H-J, Ohmuro-Matsuyama Y, Ohashi H, et al. Detection of vimentin serine phosphorylation by multicolor Quenchbodies. *Biosens Bioelectron*. 2013;40(1):17-23. Published online June 23, 2012, doi:10.1016/j.bios.2012.06.030
59. Ohashi H, Matsumoto T, Jeong H-J, Dong J, Abe R, Ueda H. Insight into the working mechanism of Quenchbody: transition of the dye around antibody variable region that fluoresces upon antigen binding. *Bioconjug Chem*. 2016;27(10):2248-2253. doi:10.1021/acs.bioconjchem.6b00217 Published Online: Sep. 26, 2016
60. Winkler JR, Gray HB. Long-range electron tunneling. *J Am Chem Soc*. 2014;136(8):2930-2939. Published online February 18, 2014, doi:10.1021/ja500215j
61. Dandliker WB, Hsu ML, Levin J, Rao BR. Equilibrium and kinetic inhibition assays based upon fluorescence polarization. *Methods Enzymol*. 1981;74 Pt C:3-28. doi:10.1016/0076-6879(81)74003-5
62. Lundblad JR, Laurance M, Goodman RH. Fluorescence polarization analysis of protein-DNA and protein-protein interactions. *Mol Endocrinol*. 1996;10(6):607-612. doi:10.1210/mend.10.6.8776720
63. Fujita S, Matsuura K. Self-assembled artificial viral capsids bearing coiled-coils at the surface. *Org Biomol Chem*. 2017;15(23):5070-5077. doi:10.1039/c7ob00998d
64. Greenfield NJ. Analysis of the kinetics of folding of proteins and peptides using circular dichroism. *Nat Protoc*. 2006;1(6):2891-2899. doi:10.1038/nprot.2006.244
65. Horne WS, Price JL, Keck JL, Gellman SH. Helix bundle quaternary structure from alpha/beta-peptide foldamers. *J Am Chem Soc*. 2007;129(14):4178-4180 Published online March 16, 2007, doi:10.1021/ja070396f

SUPPORTING INFORMATION

Additional supporting information can be found online in the Supporting Information section at the end of this article.

How to cite this article: Wack JS, Brahm K, Babel P, Dalton JAR, Schmitz K. Effect of macrocyclization and tetramethylrhodamine labeling on chemokine binding peptides. *J Pept Sci*. 2023;29(7):e3486. doi:10.1002/psc.3486